Microgrid Dynamics Characterization Using the Automated State Model Generation Algorithm

Brian B. Johnson, Ali Davoudi, Patrick L. Chapman, and Peter Sauer
Grainger Center for Electric Machinery and Electromechanics
Department of Electrical and Computer Engineering
University of Illinois at Urbana-Champaign
Urbana, USA
Email: {johnso88, davoudi2, plchapma, psauer}@illinois.edu

***Abstract*—This work presents a unified method for dynamic modeling and stability analysis of microgrid power systems. Using the automated state model generation algorithm, a state-space model of the microgrid power system is derived. The model may be used to conduct time-domain simulations and analyze system response to large transients. Additionally, eigenvalues of the system may be analyzed with respect to inverter control gains to assess small-signal stability. The proposed methodology is verified for a large-signal transient study and small-signal stability analysis using dual and single-inverter microgrid systems, respectively. The presented method is general and may be applied to balanced three-phase circuit topologies and inverter controllers without the need to derive circuit state equations.**

I. INTRODUCTION

A microgrid is a system composed of distributed energy sources located near loads of interest and capable of islanding from the main grid to provide uninterruptible power to the local loads [1]. A wide variety of energy sources including gas turbines, photovoltaics, wind turbines, and batteries may be integrated into the system. The ac energy sources in the microgrid are rectified and connected to dc buses. A voltage source inverter interfaces each dc bus with the ac microgrid bus [2], as shown in Fig. 1. Microgrids are typically implemented in mission-critical systems, and consequently their stability assessment and large-signal transient analysis is of particular interest; e.g., to study if the system is stable during large transient events such as the transition from grid-connected to islanded. Additionally, it is useful to perform small-signal stability analysis with respect to the inverter control parameters to determine the relationship between control settings and stability during small disturbances. Therefore, there has been growing interest in computer aided dynamic characterization of microgrid power systems for large signal transient study, stability analysis, and controller design [3]-[5].

Power circuit simulators generally fall into two categories: nodal-variable and state-variable based languages [6]-[7]. The former category uses circuit elements and solves nodal equations using numerical difference equations. The latter uses differential state equations established by the analyst prior to implementation. Nodal-based microgrid models using programs similar to EMTP allow for simulation of large-transients [8] but lack flexibility for small-signal stability analysis of the control system. Existing state-space models generally require a separate formulation for the power source, network, and loads [4]. Furthermore they are only valid for small disturbances.

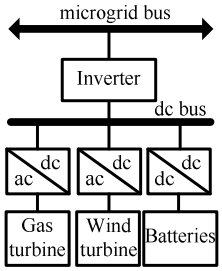

Figure 1. Power electronics interface between energy sources and microgrid bus.

The automated state model generation (ASMG) algorithm [7] combines the benefits of both nodal-variable and state-variable based approaches. This algorithm has been accelerated and improved to enhance ease of implementation and computational performance [9]. In this work, the microgrid power system is described by the pertinent branch parameters and circuit topology. The composite system state equations are established systematically, and the resulting state equations are used for large and small-signal dynamic characterizations. The proposed methodology is systematic and therefore, automatable. The state-space model may be used to derive the linearized state equations so that the eigenvalues may be analyzed at the system level [10] with respect to the inverter control parameters. This analysis will provide insight into the relationship between inverter control settings and system stability.

This work is supported by the Graduate College Fellowship and SURGE Fellowship at the University of Illinois at Urbana-Champaign.

II. MICROGRID POWER SYSTEM

The Consortium for Electric Reliability Technology Solutions (CERTS) microgrid and its associated inverter control system are considered, although the presented methods can generally be used for any type of inverter controller. Key features of the system are that each inverter operates autonomously without the need for communication between other system microsources [1], [3], [11], and the inverter system, as shown in Fig. 2, uses local measurements in addition to power and voltage commands to regulate its outputs. It will regulate either the power injected into the microgrid bus or the measured voltage during grid-connected and islanded configurations, respectively [5], [12].

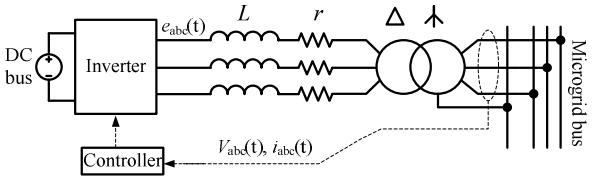

Figure 2. Inverter model and closed-loop control

A block diagram model of the controller is shown in Fig. 3 and the P, Q, and V calculations are summarized in (1), where V_{qd0} and I_{qd0} are calculated by transforming the measured quantities, V_{abc} and I_{abc}, in Figure 2 to the synchronous frame. Since each inverter is supplied by energy sources capable of satisfying the base load as well as energy storage able to supply rapid increases in power output [2], [12], the dynamics of the dc bus may be neglected for the purpose of modeling the inverter voltage output. The synchronous frequency is ω_0 and the user-defined commands are the rms voltage V^* and power P^*. Minimum and maximum power capabilities, $P_{\min}$ and $P_{\max}$, are also defined such that the physical limits of the microsource are enforced. Since the inverter switching frequency is approximately two orders of magnitude greater than the ac line frequency, the use of an average model neglecting switching ripple can be justified [13]. The outputs $|E_{\text{inv}}|$ and θ_{v} are used to control the inverter gate signals to satisfy (2).

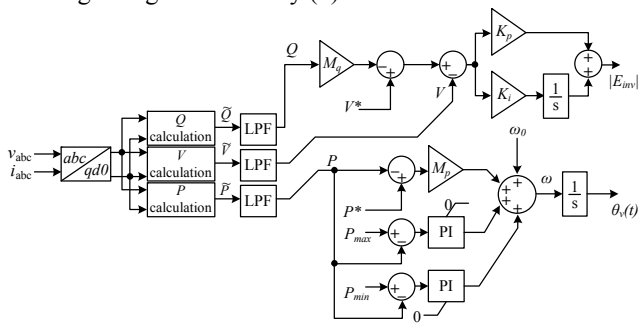

Figure 3. Inverter control block-diagram model

$$\begin{Bmatrix} P = \frac{3}{2}\left(V_d I_d + V_q I_q + 2V_0 I_0\right) \\ Q = \frac{3}{2}\left(V_d I_q - V_q I_d\right) \\ V = \sqrt{V_d^2 + V_q^2} \end{Bmatrix} \quad (1)$$

$$\begin{Bmatrix} e_a(t) = |E_{inv}| \cos\theta_v(t) \\ e_b(t) = |E_{inv}| \cos\left(\theta_v(t) - \frac{2\pi}{3}\right) \\ e_c(t) = |E_{inv}| \cos\left(\theta_v(t) + \frac{2\pi}{3}\right) \end{Bmatrix} \quad (2)$$

III. COMPOSITE SYSTEM STATE MODEL DEVELOPMENT

A. Large-signal nonlinear system development

The microgrid is represented as a collection of n nodes and b braches using a directed graph. Each branch is a variation of the elementary model shown in Fig. 4. By setting appropriate parameters to zero, a wide variety of commonly used power system circuit elements can be constructed. Using the additional capability that the voltage and current sources, e_i and j_i, can be functions of time and other variables, the voltage source inverter average model presented in section II may be represented by this elementary branch. The control block diagram in Fig. 3 is implemented using Simulink.

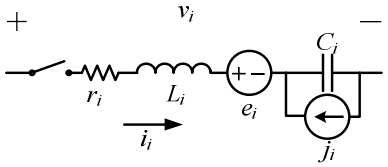

Figure 4. Elementary branch model

Defining $P_i = 1/C_i$, the parameters of each branch r_i, L_i, and P_i constitute $b \times b$ matrices $\mathbf{R_{br}}$, $\mathbf{L_{br}}$, and $\mathbf{P_{br}}$, respectively. The sources e_i and j_i form b dimensional vectors $\mathbf{e_{br}}$ and $\mathbf{j_{br}}$, respectively. The off-diagonal elements in the inductance matrices represent mutual coupling between branches and may be utilized to model three-phase transformers commonly used in microgrid power systems. The interconnected branches form the microgrid network whose structure is described by the $b \times n$ node-incidence matrix $\mathbf{A_a}$. Each column corresponding to a branch will have exactly two non-zero entries, with one equal to +1, and the other to -1. A +1 at the (i, j) entry of $\mathbf{A_a}$ indicates the connection of the positive terminal of the j^{th} branch to the i^{th} node. The -1 entry corresponds to the negative terminal connection. After row-operations, $\mathbf{A_a}$ may be expressed as (3) [7].

$$\tilde{\mathbf{A}}_{\mathbf{a}} = \begin{bmatrix} \mathbf{I}_{n-1,n-1} & \hat{\mathbf{A}}_{n-1,b-n+1} \\ \mathbf{0}_{1,n-1} & \mathbf{0}_{1,b-n+1} \end{bmatrix} \quad (3)$$

A state-space model of the microgrid may be derived using the four matrices $\mathbf{A_a}$, $\mathbf{R_{br}}$, $\mathbf{L_{br}}$, and $\mathbf{P_{br}}$. Using p to denote the differentiation operator, the state-space model of the system with no current sources is expressed using (4) and (5) [7]. Voltage sources, $\mathbf{e_{br}}$, serve as inputs to the system and the currents $\mathbf{i_x}$ and $\mathbf{q_c}$ are the state variables, where $\mathbf{q_c} = \mathbf{i_c} / p$ and $\mathbf{i_c}$ are the capacitor currents. The presented state-space model may be written succinctly as $p\mathbf{x} = \mathbf{Ax} + \mathbf{Bu}$ and $\mathbf{y} = \mathbf{Cx} + \mathbf{Du}$.

$$p\begin{bmatrix}\mathbf{q_c}\\ \mathbf{i_x}\end{bmatrix} = \begin{bmatrix}\mathbf{0} & \mathbf{M}^{\mathbf{T}}\mathbf{B_b}^{\mathbf{T}}\\ -\mathbf{L_x}^{-1}\mathbf{P_x} & -\mathbf{L_x}^{-1}\left(\mathbf{r_x} + p\mathbf{L_x}\right)\end{bmatrix}\begin{bmatrix}\mathbf{q_c}\\ \mathbf{i_x}\end{bmatrix} + \begin{bmatrix}\mathbf{0} & \mathbf{0}\\ \mathbf{0} & -\mathbf{L_x}^{-1}\mathbf{B_b}\end{bmatrix}\begin{bmatrix}\mathbf{0}\\ \mathbf{e_{br}}\end{bmatrix} \quad (4)$$

$$\begin{bmatrix}\mathbf{i_{br}}\\ \mathbf{v_{br}}\end{bmatrix} = \left[\begin{array}{c|c}\mathbf{0} & \mathbf{B_b}^{\mathbf{T}}\\ \hline \mathbf{P_{br}M} - & \left(\mathbf{r_{br}} + p\mathbf{L_{br}}\right)\mathbf{B_b}^{\mathbf{T}} - \\ \mathbf{L_{br}B_b}^{\mathbf{T}}\mathbf{L_x}^{-1}\mathbf{P_x} & \mathbf{L_{br}B_b}^{\mathbf{T}}\mathbf{L_x}^{-1}\left(\mathbf{r_x} + \mathbf{pL_x}\right)\end{array}\right]\begin{bmatrix}\mathbf{q_c}\\ \mathbf{i_x}\end{bmatrix} + \begin{bmatrix}\mathbf{0} & \mathbf{0}\\ \mathbf{0} & \mathbf{I} - \mathbf{L_{br}B_b}^{\mathbf{T}}\mathbf{L_x}^{-1}\mathbf{B_b}\end{bmatrix}\begin{bmatrix}\mathbf{0}\\ \mathbf{e_{br}}\end{bmatrix} \quad (5)$$

B. Linearization and subsequent small-signal system development

The system state equations expressed in the *abc* frame in (4) and (5) are time-varying in steady state. Therefore, Park's transformation is used to transform them to *qd0* variables so that the equilibrium values are steady-state quantities. Park's transformation from *abc* to *qd0* quantities is defined in (6).

$$\mathbf{\Gamma} = \frac{2}{3}\begin{bmatrix}\cos\theta & \cos\left(\theta - \frac{2\pi}{3}\right) & \cos\left(\theta + \frac{2\pi}{3}\right)\\ \sin\theta & \sin\left(\theta - \frac{2\pi}{3}\right) & \sin\left(\theta + \frac{2\pi}{3}\right)\\ 1/2 & 1/2 & 1/2\end{bmatrix} \quad (6)$$

By applying Park's transformation to the previous state-space model with matrix coefficients **A**, **B**, **C**, and **D**, the state-space model from (4) and (5) may be rewritten as shown in (7) and (8). Using properties of Park's transformation as summarized in [13], the matrix coefficients in (7) and (8) are time-invariant and the *qd0* state-space model has constant steady-state values.

$$p\begin{bmatrix}\mathbf{q_{c(qd0)}}\\ \mathbf{i_{x(qd0)}}\end{bmatrix} = \left[-\mathbf{\Gamma}\frac{d}{dt}\mathbf{\Gamma}^{-1} + \mathbf{\Gamma A \Gamma}^{-1}\right]\begin{bmatrix}\mathbf{q_{c(qd0)}}\\ \mathbf{i_{x(qd0)}}\end{bmatrix} + \mathbf{\Gamma B \Gamma}^{-1}\begin{bmatrix}\mathbf{0}\\ \mathbf{e_{br(qd0)}}\end{bmatrix} \quad (7)$$

$$\begin{bmatrix}\mathbf{i_{br(qd0)}}\\ \mathbf{v_{br(qd0)}}\end{bmatrix} = \mathbf{\Gamma C \Gamma}^{-1}\begin{bmatrix}\mathbf{q_{c(qd0)}}\\ \mathbf{i_{x(qd0)}}\end{bmatrix} + \mathbf{\Gamma D \Gamma}^{-1}\begin{bmatrix}\mathbf{0}\\ \mathbf{e_{br(qd0)}}\end{bmatrix} \quad (8)$$

The closed-loop system dynamics are extracted from Fig. 3, (1), (7), and (8). Since the Q, V, and P calculations shown in (1) are non-linear, the state equations must be linearized in order to extract a small-signal model at an equilibrium point.

IV. Case Studies

A. Large-signal time-domain transients

The microgrid system shown in Fig. 5, with parameters summarized in the appendix, has been verified experimentally in [14]. Here, this physical system is used to verify the large signal transient model. The loads, rated to consume a total of 18 kW, are purely resistive and connected in floating-star configurations. The grid system is modeled as an infinite bus with an equivalent impedance.

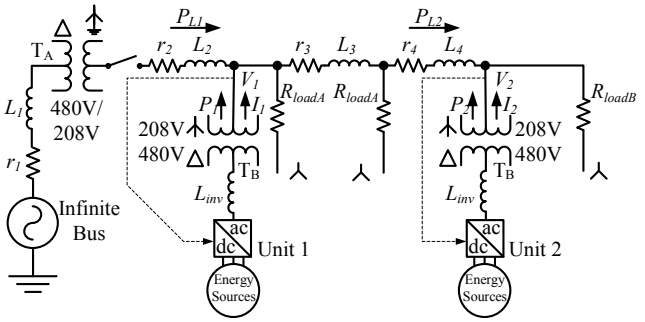

Figure 5. Dual inverter microgrid testbed

Initially, the system is grid-connected and both microsources are regulating their power output to 0.4 pu on a 15 kW base. At t = 0.25 sec, the system is islanded and the two microsources increase their power output to accommodate the total load. Simulation results, shown in Fig. 6, closely match measured results from [14]. These results verify the accuracy of the modeling technique and show that this particular system is stable during islanding.

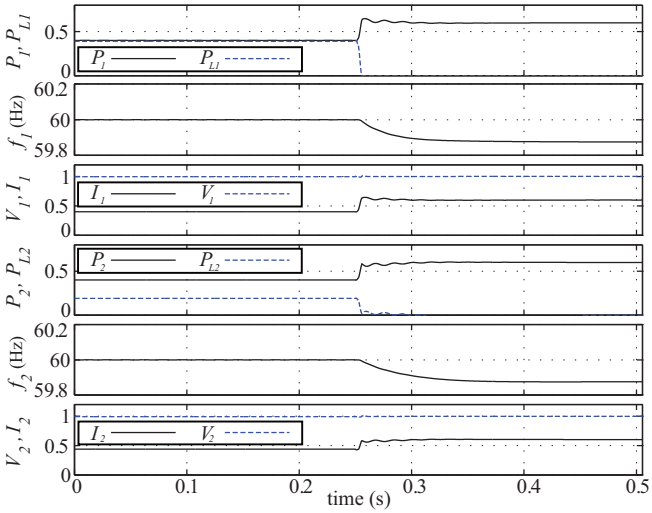

Figure 6. Transient response due to system islanding. Power, voltage, and currents are in per unit.

B. Small-signal stability analysis

The system shown in Fig. 7 is used to illustrate the relationship between the system eigenvalues and controller gains. The state variables are the inverter currents, load

currents, and the controller state variables. The nine system eigenvalues, one for each state-variable, are analyzed under varying control gains while the system is grid connected and the microsource power output is regulated to 6 kW. As each of the control gains M_p, M_q, and K_i is increased, a Hopf bifurcation is encountered and the system becomes unstable. Small-signal system stability is maintained for all values of proportional gain K_p. Table 1 summarizes the minimum gain threshold that produced unstable eigenvalues in the right half of the complex plane. The results are expressed in terms of the typically used base gains, $K_{i(0)} = 120\times10^3$, $M_{q(0)} = 0.05$, and $M_{p(0)} = 1.25\pi$.

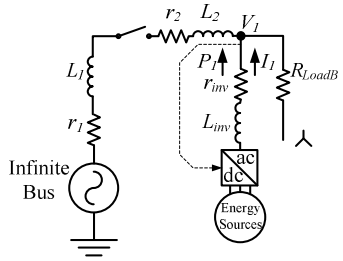

Figure 7. Single-inverter system for stability analysis

TABLE I. GAIN SETTINGS AT INSTABILITY

Parameter	Threshold gain when Re(λ) > 0
M_q	$21.25M_{q(0)}$
M_p	$151M_{p(0)}$
K_i	$4.7K_{i(0)}$

The root-locus plot corresponding to the control parameter M_q is shown in Fig. 8. For clarity, the root-locus plot contains only the eigenvalues corresponding to the $j\omega$ axis crossing. The dynamic power responses confirm the findings summarized in the root-locus plots by showing an exponentially growing output for the gain setting corresponding to right-hand plane eigenvalues as summarized in Table 1. For a slightly smaller gain, the eigenvalues are in the left-hand plane, and correspondingly, the response decays to a bounded output.

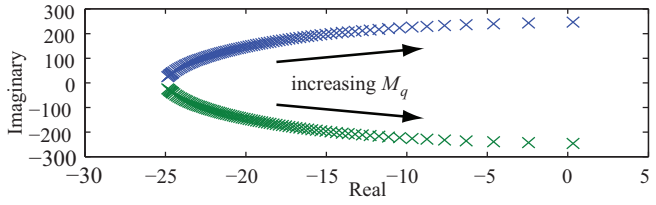

Figure 8. Root-locus plot with respect to the gain setting M_q.

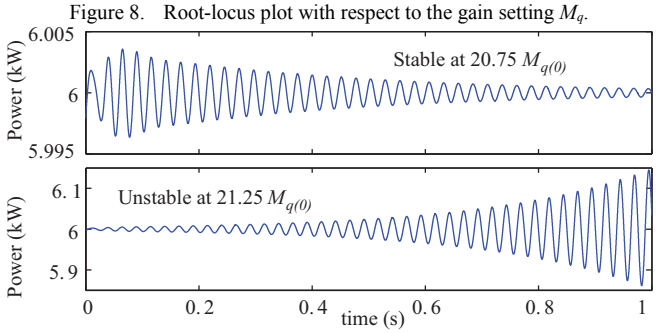

Figure 9. Stable and unstable dynamic responses.

V. CONCLUSION

A unified method for analyzing the large transient response and small-signal stability of microgrid power systems is presented. Using this method, a state-space model is derived using the node-incidence matrix and circuit parameters. The state-space model may be utilized to simulate the time-domain system response during large transients such as islanding. After performing transformations from *abc* to *qd0* variables and linearizing the state equations, the eigenvalues may be analyzed with respect to the inverter control gains. This approach is generalized for balanced 3-phase circuit topologies so that the user is not required to explicitly derive the system equations.

APPENDIX

Microgrid parameters: $r_1 = 18.9$ mΩ, $L_1 = 49.4$ μH , $r_2 = 4.20$ mΩ , $L_2 = 59.1$ μH, $r_3 = 47.4$ mΩ, $L_3 = 66.5$ μH, $r_4 = 15.8$ mΩ, $L_4 = 22.2$ μH, $L_{inv} = 5$ mH, $r_{inv} = 12.8$ mΩ, $R_{loadA} = 9.6$ Ω, $R_{loadB} = 4.8$ Ω, $r_{TA(480V)} = 30.7$mΩ, $L_{TA(480V)} = 407.4$ μH, $r_{TA(208V)} = 1.9$ mΩ, $L_{TA(208V)} = 25.5$ μH, $r_{TB(480V)} = 51.2$ mΩ, $L_{TB(480V)} = 679.1$ μH, $r_{TB(208V)} = 3.2$ mΩ, $L_{TB(208V)} = 42.4$ μH

REFERENCES

[1] R.H. Lasseter, "Microgrids," *IEEE Power Eng. Soc. Winter Meeting*, vol. 1, 2002, pp. 305–308, January 2002.

[2] H. Nikkhajoei, R. Lasseter, "Distributed generation interface to the CERTS microgrid," *IEEE Trans. Power Delivery*, vol. 24, pp. 1598-1608, July 2009.

[3] Y. Li, D. Vilathgamuwa, P. Loh "Design, analysis, and real-time testing of a controller for multibus microgrid system," *IEEE Tran. Power Electron.*, vol. 19, pp. 1195-1204, September 2004.

[4] N. Pogaku, M. Prodanovic, T. Green, "Modeling, analysis, and testing of autonomous operation of an inverter-based microgrid, " *IEEE Trans. Power Electron.,* vol. 22, no.2, pp. 613-625, March 2007.

[5] T. Green, M. Prodanovic, "Control of inverter-based micro-grids," *Electric Power Systems Research*, vol. 77, pp. 1204–1213, July 2007.

[6] A.Yildiz, B. Cakir, N. Inanc, N. Abut, "A fast simulation technique for the power electronic converters," *Applied Power Electronics Conference and Exposition*, vol.1, pp. 191-196, March 1999.

[7] O. Wasynczuk, S. Sudhoff, "Automated state model generation algorithm for power circuits and systems," *IEEE Trans. Power Syst.*, vol. 11, pp. 1951-1956, November 1996.

[8] M. Brucoli, T. Green, J.D. McDonald, "Modelling and analysis of fault behaviour of inverter microgrids to aid future fault detection," *IEEE Conference on System of Systems Eng.*, vol. 1, pp. 1-6, April 2007.

[9] L. Wang, A. Davoudi, J. Jatskevich, and P. L. Chapman, "Accelerated state-variable modeling of synchronous machine-converter systems," *IEEE International Symposium on Circuit and Systems*, vol. 1, pp. 3037-3040, May 2008.

[10] O. Wasynczuk, E. Walters, H. Hegner, "Simulation of a zonal electric distribution system for shipboard applications," *Energy Conversion Eng. Conference*, vol.1, pp. 268-273, July 1997.

[11] R. Lasseter, "CERTS microgrid," *IEEE International Conference on System of Systems Eng.*, vol. 1, pp. 1-5, April 2007.

[12] P. Piagi, R. Lasseter, "Autonomous control of microgrids," *IEEE Power Eng. Soc. General Meeting*, vol. 1, pp. 1-8, June 2006.

[13] P.C. Krause, O. Wasynczuk, S. D. Sudoff, *Analysis of Electric Machinery and Drive Systems*, 2d ed. New Jersey: IEEE Press, 2002, pp. 111-126.

[14] R. Lasseter and P. Piagi, "Control and design of microgrid components," *Power Systems Engineering Research Center*, PSERC Publication 06-03, pp. 72-103, January 2006.